Journal of ELECTRONIC MATERIALS, Vol. 47, No. 8, 2018
https://doi.org/10.1007/s11664-018-6369-4

Design Optimization of a Thermoelectric Cooling Module Using Finite Element Simulations

MUHAMMAD ABID ,[1,3] RAGNAR SOMDALEN,[2] and MARINA SANCHO RODRIGO[2]

1.—Department of Mechanical Engineering, COMSATS University Sahiwal Campus, COMSATS Road, Off GT Road, Sahiwal, Pakistan. 2.—Institut für Thermodynamik, Technische Universität Carolo-Wilhelmina zu Braunschweig, Braunschweig, Germany. 3.—e-mail: m.abid@ciitsahiwal.edu.pk

The thermoelectric industry is concerned about the size reduction, cooling performance and, ultimately, the production cost of thermoelectric modules. Optimization of the size and performance of a commercially available thermoelectric cooling module is considered using finite element simulations. Numerical simulations are performed on eight different three-dimensional geometries of a single thermocouple, and the results are further extended for a whole module as well. The maximum temperature rise at the hot and cold sides of a thermocouple is determined by altering its height and cross-sectional area. The influence of the soldering layer is analyzed numerically using temperature dependent and temperature independent thermoelectric properties of the solder material and the semiconductor pellets. Experiments are conducted to test the cooling performance of the thermoelectric module and the results are compared with the results obtained through simulations. Finally, cooling rate and maximum coefficient of performance (COP_{max}) are computed using convective and non-convective boundary conditions.

Key words: Thermoelectric cooling module, finite element simulations, soldering layer effects, experimental validation, optimized size

List of symbols

V	Applied voltage (V)
I	Applied current (A)
ΔT	Temperature difference between hot and cold side (°C)
A_P	Cross-sectional area of the semiconductor pellet (m^2)
H_P	Height of the semiconductor pellet (m)
T_c	Cold side temperature (°C)
T_h	Hot side temperature (°C)
T_{sink}	Heat sink temperature (°C)
Q_c	Heat absorbed at cold side interface (W)
Q_h	Heat released at hot side interface (W)
N	Number of thermocouples
R	Electrical resistance (Ω)
COP	Coefficient of performance
Z	Figure of merit
h	Heat transfer coefficient ($W \cdot m^{-2} \cdot K^{-1}$)
$\dot{q}_{c,max}$	Maximum heat flux at cold side ($W \cdot m^{-2}$)

Greek symbols

λ	Thermal conductivity ($W \cdot m^{-1} \cdot K^{-1}$)
λ_p	Thermal conductivity of the *p*-type semiconductor pellet ($W \cdot m^{-1} \cdot K^{-1}$)
λ_n	Thermal conductivity of the *n*-type semiconductor pellet ($W \cdot m^{-1} \cdot K^{-1}$)
α_p	Seebeck coefficient of *p*-type semiconductor element ($\mu V \cdot K^{-1}$)
α_n	Seebeck coefficient of *n*-type semiconductor element ($\mu V \cdot K^{-1}$)
ρ_p	Bulk density of the *p*-type semiconductor element ($kg \cdot m^{-3}$)
ρ_n	Bulk density of the *n*-type semiconductor element ($kg \cdot m^{-3}$)
σ	Electrical conductivity ($S \cdot m^{-1}$)

(Received November 1, 2017; accepted May 8, 2018; published online May 22, 2018)

INTRODUCTION

Worldwide energy production is mostly based on fossil fuels. With the increase in burning of fossil fuels, concentration of CO_2 has been markedly increased in the atmosphere leading to global warming. In recent years, research is focusing on the production and management of energy from antithetic renewable sources.[1–5] Among different types of alternative ways to produce energy, thermoelectricity has gained more interest, although the first thermoelectric phenomenon was observed in 1821 by Thomas Seebeck.[6] The applications of thermoelectricity can be classified into two major groups, namely, thermoelectric generators and coolers. Thermoelectric generators (TEGs) are getting more interest with the improvement of the figure of merit of thermoelectric materials.[7,8] Thermoelectric generators have been used in terrestrial and space applications for many years due to their robustness, reliability and insensitivity to radiations.[9–11] Thermoelectric waste heat recovery in automobiles has also received more interest recently because the amount of electrical energy required on-board has increased due to newly implemented features and technologies such as cabin guidance, heated seats, entertainment and other systems.[11–13] An attractive example is energy harvesting from exhaust heat in automobiles.[14–17] The exhaust heat can be converted into electricity and, therefore, the fuel consumption of the automobile can be reduced. Furthermore, a multi-parametric optimization of bismuth-telluride-based TEG is implemented to design an optimal module structure by Meng et al.[18] A 3D model coupling major relevant thermoelectric parameters is given by Ref. 19. They have also studied output power and conversion efficiency of the TEG using their developed model. In the second class of thermoelectric applications, the thermoelectric coolers (TECs), the application field ranges from the refrigeration of electronic components to air conditioning in automobiles.[20] Thermoelectric refrigerators have been used widely in portable coolers, which have been employed for carrying medical supplies for many years.[21,22] Another important application of thermoelectric refrigerators is the control of temperature for scientific and electronic systems.[23] On large scale refrigeration, thermoelectric radiant air conditioners are being used currently.[24]

The advantage of using thermoelectric cooling modules (TECMs) over conventional refrigerators lies mainly on its reliability, precise control of temperature, absence of vibrations, quietness and having no moving parts.[25,26] Recent research has focused on the miniature type thermoelectric coolers for enhancing the cooling power density in microelectronic components.[27,28] In the field of thermoelectricity, bismuth-telluride materials (Bi_2Te_3) are commonly used due to their excellent thermoelectric properties at room temperature.

Nowadays, bismuth-telluride is commonly used for conventional bulk *p*-type Bi_2Te_3-Sb_2Te_3 and *n*-type Bi_2Te_3-Bi_2Se_3 thermoelectric materials and their new dimensional forms such as quantum wells, quantum wires and quantum dots.[29–31]

In order to improve the efficiency of a thermoelectric module, whether it is used as TEG or TEC, it is necessary to analyze the influence of the different layers that constitute a thermoelectric module. Hodes[31] theoretically derived the working equation for the performance of a TECM depending on the pellet geometries. Chen et al.[32] numerically studied the performance of a 3D miniature thermoelectric cooler by varying the number of thermoelectric pairs during simulations. A theoretical relation that uses inverse problem approach to optimize the geometric structure of a TEC has been developed by Huang et al.[33] Xiaolong et al.[34] performed theoretical and experimental analysis on a low temperature thermoelectric generator system used for the recovery of waste heat. They found that the performance of the module can be increased by increasing the heat sink surface area. Cheng et al.[35] tried to maximize the cooling capacity through genetic algorithms (GAs) and proposed a method for optimizing the dimensions of the TEC legs.

It has been seen that previous researchers have focused mainly on optimizing the size of the semiconductor pellet. However, other contributing geometrical parameters, for example, a soldering layer, connecting copper strips and ceramic plates also affects its performance. Therefore, the contribution due to all constituting layers and major influencing factors on its efficiency should be addressed in order to improve the overall performance of the TECM.

The present work describes the additional factors that influence the performance of a thermoelectric cooling module and fills the knowledge gap that has not been focused in the past. Outcomes of this study will help in optimizing design of a TECM that is currently needed by the concerned thermoelectric industry. In the probed study, inevitable contact resistance problems due to soldering layers, coefficient of performance (COP), cooling rate ($\dot{q}_c$) and possible convective effects are discussed. Working performance of the semiconductor pellets are analyzed using temperature dependent and independent thermoelectric properties. In addition, experiments are performed to test the working ability of a commercially available TECM, and obtained results are compared with the simulated ones.

THEORY

Thermoelectric effect consists of three independent phenomenons, namely, Peltier, Seebeck and Thomson effects. The Peltier effect is basis for creating cooling when a voltage is applied across two terminals of a TEC. The Seebeck effect is the conversion of heat into electricity as in the case of

TEGs. The Thomson effect is the absorption/emission of heat in any conductor due to current flow when there is a temperature gradient.[36,37] The mentioned three phenomenons are interrelated through thermoelectric equations. The governing equations[38] for a single thermocouple are heat flux q and electric current density J:

$$q = \alpha \cdot T \cdot J - \lambda \cdot \nabla T \tag{1}$$

$$J = -\sigma \cdot \nabla V - \sigma \cdot \alpha \cdot \nabla T \tag{2}$$

where, α is the Seebeck coefficient, λ is the thermal conductivity and σ is the electrical conductivity of the thermocouple. ∇V, ∇T represent the electrical and temperature fields, respectively.

Production of heat due to current flow (Joule heating) can be written as,

$$Q = J \cdot (-\nabla V) \tag{3}$$

where Q represents Joule heating.

Under steady-state configurations, the following two boundary conditions may be applied:

$$\nabla \cdot q = Q \tag{4}$$

$$\nabla \cdot J = 0 \tag{5}$$

These conditions indicate that, at constant applied current, several forms of internal heating may occur in a thermoelectric sub-domain. Inserting Eqs. 1, 2 and 3 in Eq. 4 we get;

$$\begin{aligned} &\nabla \cdot [\alpha \cdot T(-\sigma \cdot \nabla V - \sigma \cdot \alpha \cdot \nabla T)] - \lambda \cdot \nabla T \\ &= (-\sigma \cdot \nabla V - \sigma \cdot \alpha \cdot \nabla T) \cdot (-\nabla V) \end{aligned} \tag{6}$$

Inserting Eq. 2 in Eq. 5 gives,

$$\nabla \cdot (-\sigma \cdot \nabla V - \sigma \cdot \alpha \cdot \nabla T) = 0 \tag{7}$$

For a more simplified solution in simulating software, Eqs. 6 and 7 are transferred to the weak form by multiplying each side with a test function and subsequently applying an integral over the computational sub-domain Ω. Consequently, the two main equations can be written as:

$$q \cdot \text{test}(\nabla T) + Q \cdot \text{test}(T) = 0 \tag{8}$$

$$J \cdot \text{test}(\nabla V) = 0 \tag{9}$$

The COP for a thermoelectric cooler is defined as,

$$\text{COP} = \frac{\dot{Q}_c}{P} \tag{10}$$

where P is the applied electrical power and ($\dot{Q}_c$) is the heat flow rate entering to the cold side of the ceramic substrate from the ambient air.

Material Properties

Bismuth-telluride alloys are mostly used as semiconductor materials in thermoelectric modules because of their high figure of merit at 300 K.[39] In this work, the selected semiconductor materials for the n- and p-type pellets are bismuth-telluride alloys supplied by the company Ferrotec NORD. Interconnection of the semiconductor pellets and copper conductor are made by soldering. Best material selection for enhancement of the operating temperature and the performance of the soldering material has already been discussed by many authors.[40,41] Recent research is focusing on lead-free solders and new gluing materials.[41,42] Efforts are being made to increase the electrical and thermal conductivities, fatigue strength and good adhesion to the surface. Furthermore, the soldering material should have similar expansion coefficient as that of the substrate. Typically, $Sn_{95.3}Ag_4Cu_{0.7}$, $Sn_{96.5}Ag_3Cu_{0.5}$ and $Sn_{97.3}Cu_{0.7}$ are widely used as lead-free solders.[37] In this work $Sn_{95.3}Ag_4Cu_{0.7}$ has been used as a soldering material.

Ceramic plates at the top and bottom surfaces of the TEC are usually made of aluminum oxide (Al_2O_3). These plates electrically isolate the TECM from the object to be cooled and provide mechanical strength to the module. In this work, aluminum oxide (Al_2O_3) is selected for the ceramic substrate because of its optimal cost and performance ratio and widespread use in TECMs.[43] Aluminum nitride (AlN) is also used as a ceramic substrate due to its higher thermal conductivity and lower thermal expansion coefficient; however, it is more expensive as compared to Al_2O_3.

Electrical conductors provide serial electrical connection between pellets and the leading wires. For most of the TECMs, the conductors are made of copper because of good electrical and thermal conductance. Thermoelectric properties of p- and n-type semiconductor elements, solder layer, ceramic plates and copper are given in Table I.

WORKING STRATEGY

The presented research work is performed in three steps. In the first step, experiments are conducted on a typical TECM having dimensions $2.4 \times 2.4 \times 2\ \text{mm}^3$ (provided by the company Ferrotec-NORD) and the temperature difference between its hot and cold surfaces is measured for different values of applied voltage. In the second step, experimental results are justified by using numerical simulations while keeping similar boundary conditions as are used during experiments. In the third and final step, design optimization of a single TEC/TECM is formulated by running numerical simulations on eight geometries using different boundary conditions.

Table I. Thermoelectric and physical properties of *n*- and *p*-type semiconductor pellets solder layer, ceramic sheet, and copper at 300 K

Properties	$\alpha\ (\mu \mathbf{V \cdot K^{-1}})$	$\lambda\ (\mathbf{W \cdot m^{-1} \cdot K^{-1}})$	$\sigma\ (\mathbf{S \cdot m^{-1}})$	$c_p\ (\mathbf{J \cdot kg^{-1} \cdot K^{-1}})$	$\rho\ (\mathbf{kg \cdot m^{-3}})$	Ther.exp. co. $(\mathbf{10^{-6} \cdot K^{-1}})$
p-type semiconductor[44,45]	200.652	1.387	1.03×10^5	154.4	7740	7.50
n-type semiconductor[44,45]	− 205.51	1.397	9.47×10^4	154.4	7740	7.50
$Sn_{95.3}Ag_4Cu_{0.7}$[41,45]	− 1.20	64.40	8.03×10^6	262.0	7400	23.3
Al_2O_3[43,45]	–	35.00	1.0×10^{-14}	775.0	3800	5.00
Cu[43,45]	6.50	391.1	5.91×10^7	393.0	8920	17.0

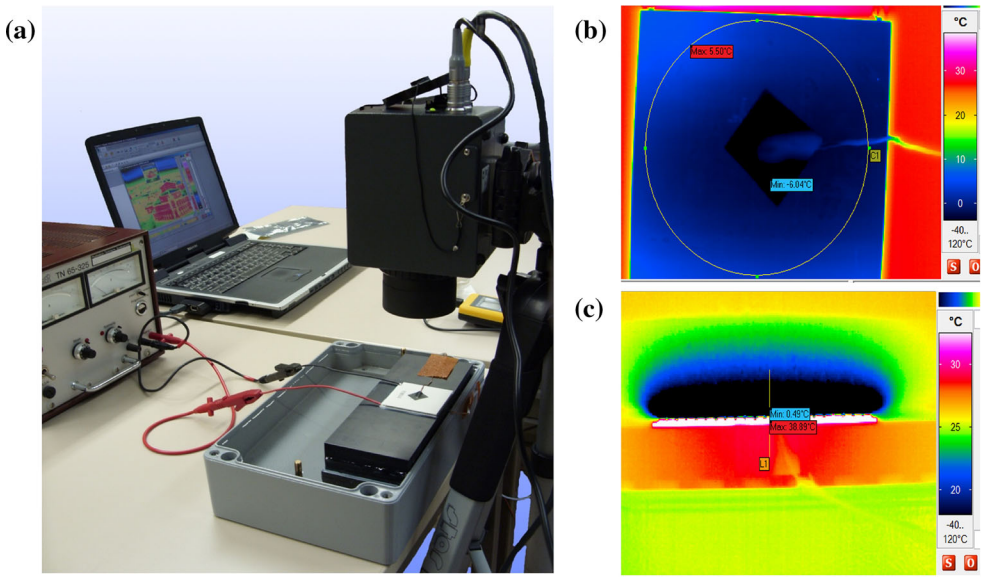

Fig. 1. Experimental results: (a) experimental setup, (b) infrared picture from the top of the module during cooling, and (c) infrared picture from the side of the module.

Experimental Setup and Results

In order to validate the simulated work, experiments are conducted under steady state conditions for the mentioned TECM. Hot side of the module is connected to a set of fins (heat sink) kept in a box filled with cold water. Experimental setup for investigating temperature increase is shown in Fig. 1. Figure 1a shows the experimental setup used to measure the temperature rise within the cooling module through an infrared camera, where Fig. 1b and c shows temperature rise at top and at sides of the module, respectively. In addition, to verify the infrared camera results, two thermocouples (K-type) were also employed to measure the top and bottom side temperatures of the module. LabVIEW 2010 software is used for displaying and saving the measured data from the thermocouples.

Experiments are performed at three different applied voltages and temperature rise is recorded between hot and cold sides of the TECM. Results show that by increasing applied voltage, temperature difference between hot and cold ceramic plates also increases. A comparison of experimental and simulation results are shown in Table II. It can be noted that for the same values of applied voltage or current, the temperature difference (ΔT) between the hot and cold side of the thermocouple was a bit higher in the simulations as compared to the experimental values (see Table II). The difference can be explained in terms of accuracy of the thermoelements employed for temperature measurements. For this work, type-K thermoelements having accuracy of ± 1 K are used. In addition, inevitable contact resistance and noise also affected the experimental values. Nevertheless, experimental values are very close to the simulation results which show the validity of the simulated results.

Thermoelectric Cooler Geometry

A single thermocouple consists of two branches: a *p*-type semiconductor pellet with positive Seebeck

Table II. Comparison of experimental and simulated results

	Experimental results			Simulated results			
Voltage (V)	T_h (K)	T_c (K)	ΔT(K)	T_h (K)	T_c (K)	ΔT(K)	**% Error**
1.85	290.29	276.39	13.90	290.29	274.75	15.54	11.78
3.65	298.75	271.13	27.62	298.75	269.23	29.52	06.88
5.45	310.69	269.78	40.91	310.69	268.10	42.59	04.11
7.28	323.70	269.91	53.79	323.70	268.85	54.85	01.97

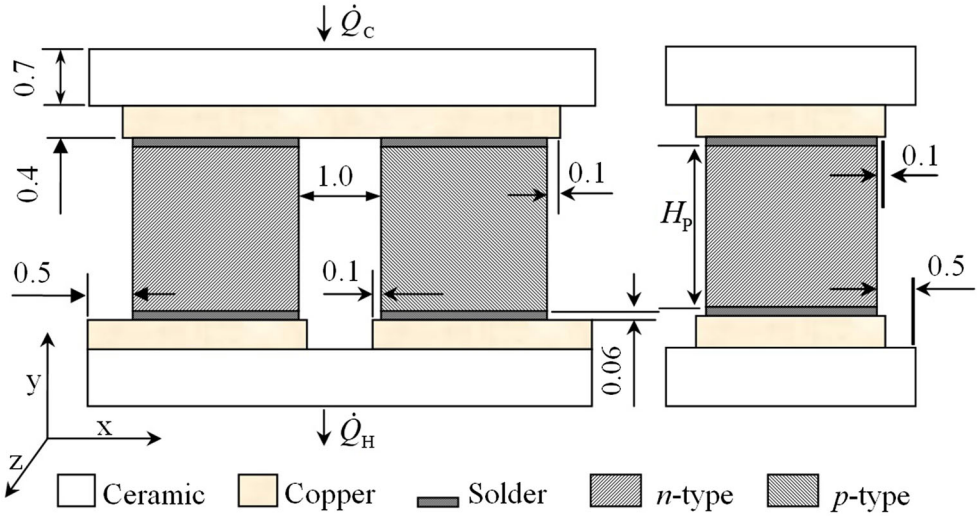

Fig. 2. Geometry of a single thermocouple with variable semiconductor pellet height (H_P) Hand cross-sectional area (A_P) (all dimensions are in mm).

coefficient and an *n*-type semiconductor pellet with negative Seebeck coefficient. A metal piece (copper) interconnects the two pellets through soldering. The metal conductors are electrically isolated from the body to be cooled by means of ceramic plates. The soldering layer residing between the electrical conductor and the semiconductor pellet acts as a contact resistance and decreases maximum heat pumping capacity of the whole module. Figure 2 illustrates a 2D sketch diagram of a single thermocouple, whereas, in simulation software, a 3D single stage TEC is analyzed.

SIMULATION RESULTS

In this research work, COMSOL Multiphysics 4.2a is used for the finite element simulations. Used software has the ability to couple the thermal and electrical aspects allowing users to simulate both phenomenon simultaneously. Following initial and boundary conditions are applied during the simulations;

1. All the simulations are performed under steady state conditions.
2. *n*- and *p*-type pellets have similar cross sectional area (AP) and height (HP).
3. Thermoelectric pellets (*p*- and *n*-type) are connected electrically in series and thermally in parallel.
4. Radiation heat transfer is neglected.
5. To achieve the maximum temperature difference across the thermocouple/module, boundary conditions are set in such a way that there is no heat flow from the cold side (i.e., Q_c = 0 W) and the initial temperature of the cold and hot side of the module is set at $T_c = T_h$ = 298.15 ,K whereas the temperature of the heat sink (cold water) is kept constant at T_{sink} = 283.15 K.

Figure 3 shows temperature distribution at the surface of a thermocouple for a 2.4 × 2.4 mm^3 geometry and an applied voltage of 0.12 V.

Effect of Temperature Dependent Material Properties

Temperature dependent and independent properties (at 20°C) for *n*- and *p*-type semiconductor materials are

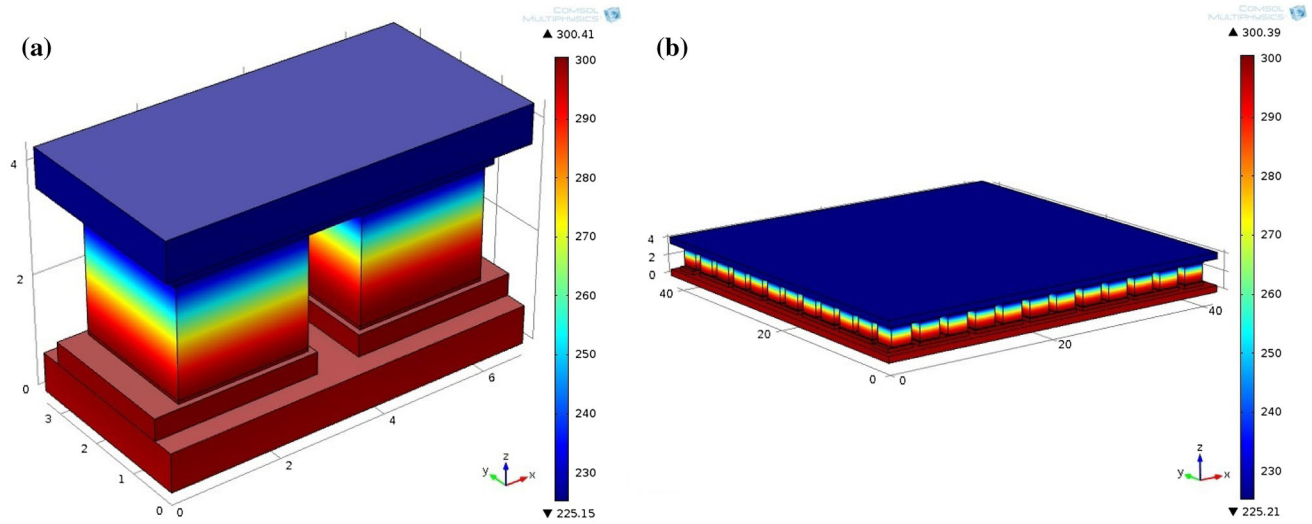

Fig. 3. (a) Temperature distribution in a single thermocouple at ΔT_{max}. (b) Distribution of temperature in a TEM with 36 thermocouple pairs at ΔT_{max}.

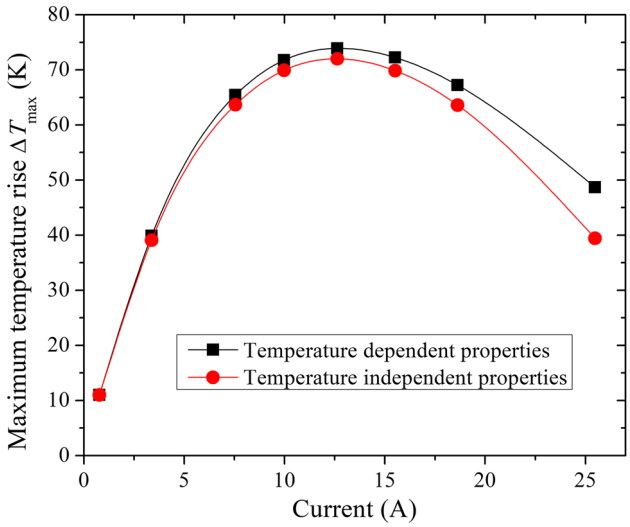

Fig. 4. Maximum temperature difference in a single thermoelectric couple by using temperature dependent and independent semiconductor pellet properties.

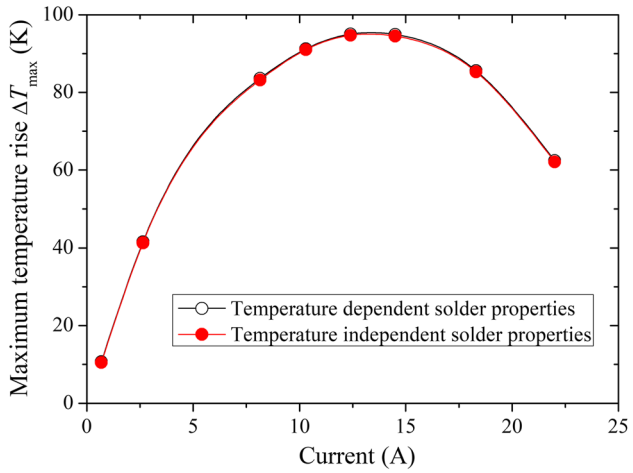

Fig. 5. Maximum temperature rise in a single thermoelectric pellet obtained after using temperature dependent and temperature independent values of the soldering material.

taken from Refs. 44 and 45. Findings of these simulations are shown in Figs. 4 and 5. Conclusion of this analysis shows that temperature dependent properties have only influence on the performance of the semiconductor pellets. More temperature rise is observed for those simulations in which temperature dependent thermal properties of the semiconductor pellets are used. Similar trend is also quoted by Wang et al. They worked on a three-dimensional numerical modeling of a miniature type thermoelectric module.[46]

In addition, parametric study of a thermoelectric generator using variable material properties has been discussed by Meng et al.[47] They have developed a 3D numerical model to investigate the thermoelectric generator performance and calculated the pellet temperature rise with respect to different convective heat transfer coefficients.

Results of this work show that there is little influence on the cooling performance of the thermocouple by using temperature dependent properties of the soldering ($Sn_{95.3}Ag_4Cu_{0.7}$) material. Therefore, one can simulate solder effect with temperature independent properties for similar size of geometries. Nevertheless, this analysis should be repeated each time when a different soldering material is used.

SIMULATION RESULTS FOR AN OPTIMIZED DESIGN

Finite element simulations are performed on eight different geometries of a single thermocouple.

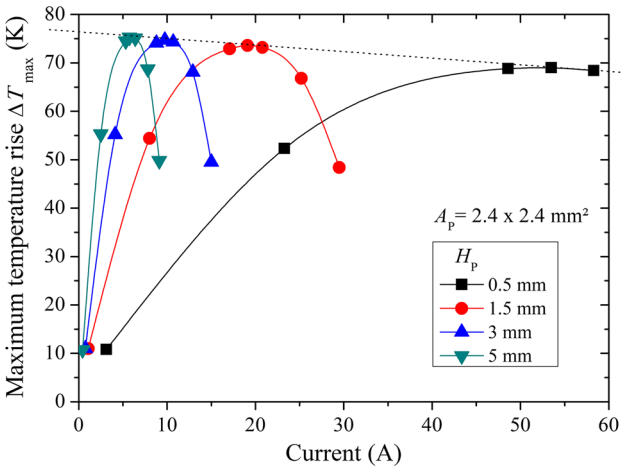

Fig. 6. Temperature increase between ceramic substrates versus applied current for variable pellet heights.

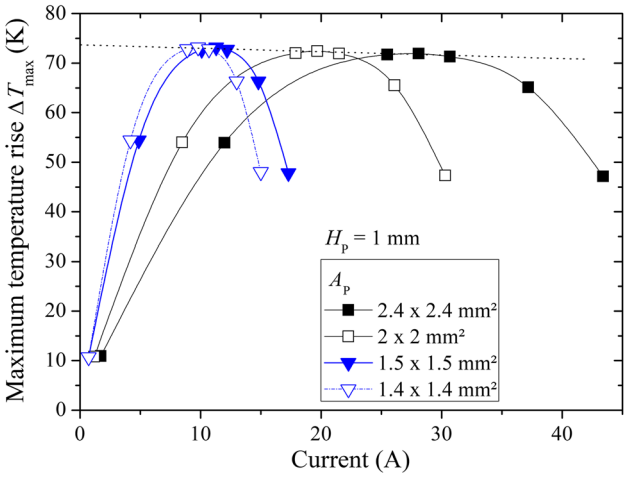

Fig. 7. Temperature increase between the ceramic substrates versus applied current for variable cross-sectional area of the pellets.

During first run, four different semiconductor pellet heights (H_P) are analyzed while keeping the cross-sectional area constant to 2.4 × 2.4 mm^2. In the second run, four different cross-sectional areas (A_P) of semiconductor pellets are analyzed while keeping the height constant to 1 mm.

Where, H_P includes four different values of 0.5 mm, 1.5 mm, 3 mm and 5 mm, and A_P includes four different cross-sectional areas of 2.4 × 2.4 mm^2, 2.0 × 2.0 mm^2, 1.5 × 1.5 mm^2 and 1.4 × 1.4 mm^2. Simulation results for maximum temperature rise that can be achieved by using the mentioned eight different geometries of the semiconductor pellet are shown in Figs. 6 and 7.

Maximum Temperature Increase due to Change in Pellet Height

During the first test, four semiconductor pellets whose heights are different, but have the same cross-sectional area are simulated. Boundary

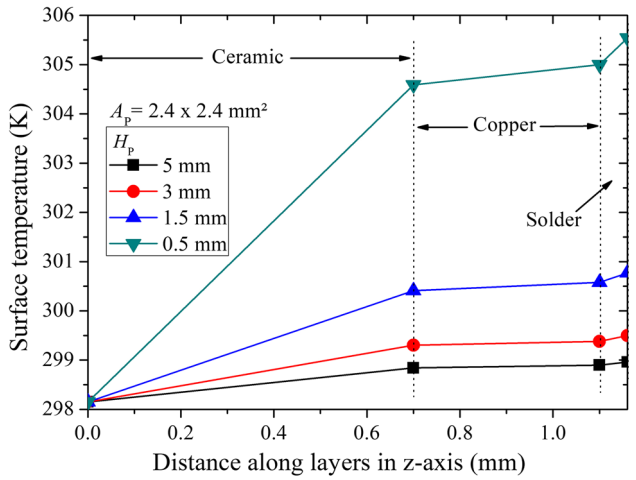

Fig. 8. Local temperature rise along the thermocouple at ΔT_{max} conditions for different pellet heights.

conditions for this analysis are applied in such a way that the hot side temperature is kept constant at T_h = 298.15 K and applied voltage difference is fixed at (ΔV = 0.12 V) between the two terminals.

Figure 6 shows maximum temperature rise in the mentioned four geometries against applied current. Results show that higher temperature difference is obtained by increasing height of the semiconductor element. This might be because of the fact that less joule heat reaches at the cold side which results higher temperature difference across the semiconductor pellet. In addition, it can be seen that for the highest pellet, the peak value current (I_{max}) is minimum.

Maximum Temperature Increase due to Change in Pellet Cross-Sectional Area

The second step of the simulations is to observe the temperature increase in the TEC by changing the cross-sectional area of the semiconductor pellet while keeping the height constant to H_P = 1 mm. Results of the mentioned four pellet cross-sectional areas show that the temperature difference between hot and cold side of the TEC increases by decreasing the cross-sectional area of the semiconductor elements, as shown in Fig. 7.

From these results it can be concluded that the temperature difference between hot and cold ceramic plates of a TEC/TECM can be increased by increasing height to cross-sectional area ratio (H_P/A_P). Results at the point of maximum temperature rise for each H_P and A_P are important in the selection of an appropriate pellet size for the thermoelectric industry.

Local temperature rise along the length of the module at maximum temperature rise conditions is shown in Fig. 8. Maximum temperature conditions are achieved by applied boundary conditions of hot ceramic side fixed at T_h = 298.15 K, Q_c= 0 W, and

Table III. Temperature rise between upper and lower ceramic substrates for selected semiconductor geometries with and without solder at constant applied voltage of 0.12 V

Geometry (mm^3)	ΔT_{max} (K)
$1.4 \times 1.4 \times 0.5$	71.05
$1.4 \times 1.4 \times 0.5$ (without solder)	71.54
$1.4 \times 1.4 \times 2.0$	74.57
$1.4 \times 1.4 \times 2.0$ (without solder)	74.70
$2.4 \times 2.4 \times 0.5$	68.63
$2.4 \times 2.4 \times 0.5$ (without solder)	69.06
$2.4 \times 2.4 \times 2.0$	73.91
$2.4 \times 2.4 \times 2.0$ (without solder)	74.03

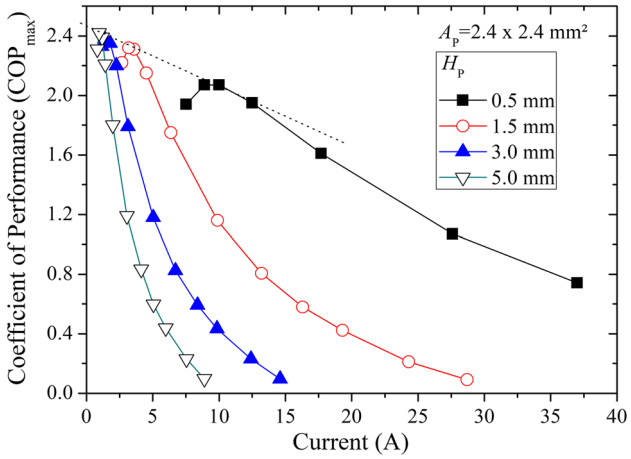

Fig. 9. Coefficient of performance versus applied current.

voltage at 0.12 V. It can be seen that the ceramic plate at hot side of the module, copper connector and the solder element plays an important role in decreasing the temperature rise at both ends. Particularly, for smaller pellet heights temperature drops rapidly.

Influence of Soldering Layer

A unified body of a TECM is not possible because of the four different types of material layers used during its construction. Therefore, all four materials must be attached by soldering or gluing. The soldering layer between the interconnecting metals and the semiconductor branches may influence the thermoelectric cooling or power generating performance.

In previous sections, all the analyzed geometries have 60 μm thickness of the soldering layer. This thickness, however, is a small portion of the total volume of the module and therefore may not adversely affect the performance of the TEC. Nevertheless, performance of the TEC must be checked using changed thickness of the soldering material.

For this purpose eight geometries were chosen out of which four have a soldering layer (0.5 mm and 2 mm thick) and four did not. Table III shows the results of maximum temperature increase for the selected geometries. It can be seen that for the selected soldering material and its thicknesses, there is about 0.7% decrease in the temperature by considering soldering layer. We can conclude that user may disregard any effect due to soldering layer provided the solder thickness is within the simulated range.

Coefficient of Performance

COP_{max} for four pellet geometries is calculated under the same conditions as used for the analysis of the maximum cooling rate in the previous section. Figure 9 shows a plot of COP_{max} versus applied current for each of the four values of H_P. Results indicate that COP_{max} increases by increasing semiconductor pellet height (H_P). Table IV illustrates the rate of heat flow at hot and cold side and the COP_{max} for above mentioned four geometries.

When the entire module is analyzed, it is observed that maximum heat flux at the cold side ($\dot{q}_{c,max}$) and ΔT_{max} are mainly dependent on the semiconductor geometry. The semiconductor geometry should be selected according to the requirements of the application where the TECM has to be used. Table V summarizes some important findings of the simulations.

Influence of Natural Convection

In some of the industrially manufactured modules, the peripheries of the TECMs are exposed to convection during application, while in other ones peripheries are covered by a polymer sheet that works as an insulator. In the following section, influence of the convection on the performance of a single TEC is analyzed. Heat transfer due to convection can be described by Newton's law of cooling:

$$\frac{d\dot{Q}_{conv}}{dt} = hA(T_s - T_\infty) \tag{11}$$

where h is the heat transfer coefficient, A is the heat transfer surface area (i.e., contact surface), T_s is the temperature of the solid surface and T_∞ is the temperature of the flowing fluid/ambient. Heat transfer coefficient (h) depends on the flow type, solid geometry, and wall and fluid properties. In this work, natural convection along the peripheries of a single TEC is considered. Here, value of h is kept constant along all the surfaces as there exists no empirical correlation regarding geometry comparable to the modeled one. Chosen semiconductor geometry for this analysis is $2.4 \times 2.4 \times 2.0$ mm^3.

To determine the convective effects on heat flux density, simulations are performed when there is

Table IV. COP_{max} for four different semiconductor pellet heights

H_P (mm)	Voltage (V)	I (A)	Q_c (W)	Q_h (W)	COP_{max}
0.5	0.023	8.98	0.43	0.63	2.08
1.5	0.023	3.16	0.17	0.24	2.32
3.0	0.023	1.60	0.09	0.12	2.38
5.0	0.023	0.96	0.05	0.07	2.41

Table V. Summary of results: performance dependence of a thermocouple on H_P and A_P values

$\uparrow H_P$ (A_P constant)	$\Rightarrow$	$\uparrow \Delta T_{max}$, $\uparrow COP_{max}$ $\downarrow \dot{q}_{c,max}$,$\downarrow I_{max}$
$\uparrow A_P$ (H_P constant)	$\Rightarrow$	$\downarrow \Delta T_{max}$, $\downarrow COP_{max}$ $\uparrow \dot{q}_{c,max}$,$\uparrow I_{max}$

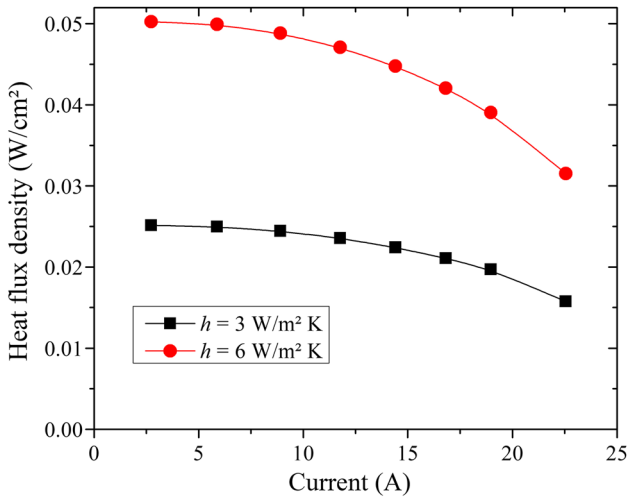

Fig. 10. Cooling rate per unit area versus applied current for two different convection values at $\Delta T = 60$ K.

maximum temperature increase, i.e., $\Delta T = 60$ K across the TEC. Convection heat transfer is simulated with two values of heat transfer coefficients, i.e., $h = 3\ W \cdot m^{-2} \cdot K^{-1}$ and $h = 6\ W \cdot m^{-2} \cdot K^{-1}$. Results are shown in Fig. 10.

Similar work has been done by Wang et al.[46] They used a theoretical model on a miniature type thermoelectric cooler and analyzed cooling rate at the cold side of the TEC using four different heat transfer coefficients whose values range from $0\ W \cdot m^{-2} \cdot K^{-1}$ to $200\ W \cdot m^{-2} \cdot K^{-1}$. Their results conclude that cooling rate increases by increasing the heat transfer coefficient value (h).[46] The tested module was analyzed at $\Delta T = 60$ K. Our results also show a similar trend, i.e., cooling rate from cold side surface increases by increasing heat transfer coefficient value. Figure 10 represents the variation of the heat flux density (cooling rate) versus applied current at $\Delta T = 60$ K. It is also noted that, as the applied current increases, more Joule heating is produced in the TEC and flows towards cold side of the TEC which reduces the maximum temperature rise and ultimately decreases the cooling capacity.

CONCLUSIONS

In the presented research work, simulations, as well as experiments are performed to optimize the working ability of a thermoelectric cooling module. Results show that temperature dependent material properties of semiconductor pellets should be used during simulations while studying thermoelectric phenomenon. Solder type and the convection boundaries may also affect significantly the performance of the thermoelectric devices. Results show that a higher temperature increase across a TECM is obtained by increasing height to cross-section area (H_P/A_P) ratio of the semiconductor pellet. Cooling rate can be increased either by increasing the applied current or by decreasing the semiconductor pellet height. Likewise, the coefficient of performance of a thermoelectric couple can be increased by increasing semiconductor pellet height. Furthermore, convection can increase or decrease the cooling rate depending on the temperature difference between hot and cold ceramic plates. Concerned thermoelectric industry can reduce manufacturing costs of TECMs by considering outcomes of this research work.

ACKNOWLEDGEMENTS

Author is thankful to the “Deutsche Bundesstiftung Umwelt” for financially supporting this work.

REFERENCES

1. S. Riffat and X. Ma, *Appl. Therm. Eng.* 23, 913 (2003).
2. J.C. Bass, D.T. Allen, S. Ghamaty, and N.B. Elsner, in *20th IEEE Semiconductor Thermal Management and management symposium* (2004).
3. H.J. Goldsmid, *Introduction to Thermoelectricity* (Springer Series in Materials Science, 2009).
4. M.T. Terry, *Semiconductors and Semimetals. Recent Trends in Thermoelectric Materials Research* (London: Academic Press, 2000).
5. Y. Pan, B. Lin, and J. Chen, *Appl. Energy* 84, 882 (2007).
6. M.T. Terry and M.A. Subramanian, *Thermoelectric Materials, Phenomena, and Applications: A Bird’s Eye View* (Cambridge: MRS Bulletin, 2006).
7. A. Kyunghan, L. Changpeng, U. Ctirad, and G.K. Mercouri, *Chem. Mater.* 21, 1362 (2009).

8. X. Yukun, C. Guoxin, Q. Haiming, W. Menglei, X. Zhepeng, J. Jun, X. Jingtao, J. Haochuan, and X. Gaojie, *J. Mater. Chem. A* 2, 8512 (2014).
9. Y. Jihui and C. Thierry, *Mater. Res. Soc.* 3, 224 (2006).
10. M. Fankai, C. Lingen, and S. Fengrui, *Cryogenics* 49, 57 (2009).
11. H.L. Kong and J.K. Ook, *Int. J. Heat Mass Transfer* 50, 1982 (2007).
12. R.R. Chethan, S.R. Shrikantha, D. Vijay, and R. Karthikeyan, *Int. J. Sci. Res.* 2, 242 (2013).
13. Y. Kazuaki and S. Ali, *J. Mater. Res.* 27, 1211 (2012).
14. K. Takashi, K. Kazuhisa, M. Kazuya, K. Takeshi, K. Hiromasa, H. Hirokuni, M. Hidetoshi, and F. Akio, *J. Electron. Mater.* 43, 2405 (2014).
15. P. Dipak and R.R. Arakerimath, *Int. J. Res. Aeron. Mech. Eng.* 1, 1 (2013).
16. N.R. Kristiansen, G.J. Snyder, H.K. Nielsen, and L. Rosendahl, *J. Electron. Mater.* 41, 1024 (2012).
17. C.R. Kumar, A. Sonthalia, and G. Rahul, *Ther. Sci.* 15, 1011 (2011).
18. J.H. Meng, X.X. Zhang, and X.D. Wang, *Energy* 71, 367 (2014).
19. J.H. Meng, X.X. Zhang, and X.D. Wang, *J. Power Sources* 245, 262 (2014).
20. D.M. Rowe, *Int. J. Innov. Energy Syst. Power* 1, 13 (2006).
21. A. Attar, H. Lee, and W. Sean, *J. Electron. Mater.* 43, 2179 (2014).
22. Z. Dongliang and T. Gang, *Appl. Therm. Eng.* 66, 15 (2014).
23. B.J. Huang, C.J. Chin, and C.L. Duang, *Int. J. Refrig.* 23, 208 (2000).
24. S. Limei, T. Zhilong, H. Qiang, T. Cheng, and C. Huanxin, *Appl. Therm. Eng.* 112, 688 (2017).
25. O. Sullivan, M.P. Gupta, S. Mukhopadhyay, and S. Kumar, *J. Electron. Packag.* 134, 1 (2012).
26. S.P. Gajendra, B.T. Abhijeet, and K.S. Babalu, in *International Conference on Advances in Engineering and Technology* (2014), pp. 28–33.
27. R.E. Simons, M.J. Ellsworth, and R.C. Chu, *ASME J. Heat Trans.* 127, 76 (2005).
28. N. Peranio, Structural, chemical, and thermoelectric properties of Bi_2Te_3 Peltier materials: bulk, thin films and superlattices. Ph.D. thesis. Von der Fakultät für Mathematik und Physik der Eberhard-Karls-Universität zu Tübingen (2008).
29. K. Park, S.W. Nam, and C.H. Lim, *Intermetallics* 18, 1744 (2010).
30. H.J. Goldsmid, *Materials* 7, 2577 (2014).
31. M. Hodes, *IEEE Trans. Comp. Packag. Technol.* 30, 50 (2007).
32. W.H. Chen, C.Y. Liao, and C.I. Hung, *Appl. Energy* 89, 464 (2012).
33. Y.X. Huang, X.D. Wang, C.H. Cheng, and D.T. Lin, *Energy* 59, 689 (2013).
34. X.L. Gou, H. Xiao, and S.W. Yang, *Appl. Energy* 87, 3131 (2010).
35. Y.H. Cheng and W.K. Lin, *Appl. Therm. Eng.* 25, 2983 (2005).
36. M. Hodes, *IEEE Trans. Compon. Packag. Technol.* 28, 219 (2005).
37. D.M. Rowe, *Handbook of Thermoelectrics* (Boston: CRC Press, 1995).
38. H.S. Lee, *Energy* 56, 61 (2013).
39. C. Godart, A.P. Goncalves, E.B. Lopes, and B. Villeroy, *NATO Science for Peace Security Series B: Physics and Biophysics* (2009), pp. 19–50.
40. T.Y. Lin, C.N. Liao, and T.W. Albert, *J. Electron. Mater.* 1, 153 (2012).
41. S. Mhiaoui, Physical properties of lead free solders in liquid and solid state. Ph.D. thesis. Von der Fakultät für Naturwissenschaften der Technischen Universität Chemnitz (2007).
42. M. Picard, S. Turenne, D. Vasilevskiy, and R.A. Masut, *J. Electron. Mater.* 7, 2343 (2013).
43. W.H. Chen, C.C. Wang, C. Hung, C.C. Yang, and R.C. Juang, *Energy* 64, 287 (2014).
44. H. Olle and R. Andersson, *J. Electron. Mater.* 6, 2247 (2014).
45. K.S. Kim, K. Suganuma, J.M. Kim, and C.W. Hwang, *Miner. Met. Mater. Soc.* 6, 39 (2004).
46. X.D. Wang, Y.X. Huang, C.H. Cheng, D. Lin, and C.H. Kang, *Energy* 47, 488 (2012).
47. J.H. Meng, X.X. Zhang, and X.D. Wang, *Int. J. Heat Mass Transfer* 80, 227 (2015).